Liver Macrophage Function is Guided by Micro-environment rather than Origin.

Lynette Beattie[1,3], Amy Sawtell[1], Jason Mann[1], Teija CM Frame[3], Bianca Teal[3], Fabian de Labastida Rivera[3], Najmeeyah Brown[1], Katherine Walwyn-Brown[1], John W.J. Moore[1], Sandy MacDonald[2], Eng-Kiat Lim[1], Jane E Dalton[1], Christian R Engwerda[3], Kelli P MacDonald[3] and Paul M. Kaye[1]*

Short Title: Comparison of yolk sac- and bone marrow-derived Kupffer cells.

Affiliations:

[1]Centre for Immunology and Infection, Hull York Medical School and Dept. of Biology, University of York, York, YO10 5DD, UK.

[2] Biosciences Technology Facility, Dept. of Biology, University of York, York, YO10 5DD, UK.

[3]QIMR Berghofer Medical Research Institute, 300 Herston Rd, Herston, Queensland, Australia, 4006.

Grant Support: This work was funded by the UK Medical Research Council (Grant #G0802620) and the Australian National Health and Medical Research Council (Grant #APP1105817).

Correspondence to: Paul Kaye, Centre for Immunology and Infection, Hull York Medical School and Dept. of Biology, University of York, York, YO10 5DD, UK. paul.kaye@york.ac.uk. Ph: +44 1904 328840 Fax: +44 1904 328844

Transcript Profiling: Gene expression data to be submitted to EBI Array Express upon acceptance.

Disclosures: The authors declare no financial, professional or personal conflicts of interest.

Author Contributions: LB conceived and designed the study, performed experiments, analysed data and wrote the manuscript. AS, JM, TCMF, BT, FLR, KW-B, JWJM, EKL and JED performed and analysed some of the experiments. SM analysed the gene expression array data. CRE and KPM contributed to data analysis. PMK conceived and designed the study, analysed data, and wrote the manuscript.

Plain English Summary: Liver macrophages play a major role in the control of infections in the liver and in the pathology associated with chronic liver diseases. It was recently shown that liver macrophages can have two different origins, however, the extent to which these populations are functionally distinct remains to be fully addressed. Our study demonstrates that whilst liver macrophages share many features in common, regardless of their origin, some subtle differences in function exist.

Abstract:

Background and aims: Kupffer cells (KCs), the resident tissue macrophages of the liver, play a crucial role in the clearance of pathogens and other particulate materials that reach the systemic circulation. Recent studies have identified KCs as a yolk sac-derived resident macrophage population that is replenished independently of monocytes in the steady state. Although it is now established that following local tissue injury, bone-marrow derived monocytes may infiltrate the tissue and differentiate into macrophages, the extent to which newly differentiated macrophages functionally resemble the KCs they have replaced has not been extensively studied.

Methods and results: Here we show using intravital microscopy, morphometric analysis and gene expression profiling that bone marrow derived "KCs" accumulating as a result of genotoxic injury resemble, but are not identical to their yolk-sac (YS) counterparts. An ion homeostasis gene signature, including genes associated with scavenger receptor function and extracellular matrix deposition, allows discrimination between these two KC populations. Reflecting the differential expression of scavenger receptors, YS-derived KCs were more effective at accumulating Ac-LDL, whereas surprisingly they were poorer than BM-derived KCs when assessed for uptake of a range of bacterial pathogens. The two KC populations were almost indistinguishable in regard to i) response to LPS challenge, ii) phagocytosis of effete RBCs and iii) their ability to contain infection and direct granuloma formation against *Leishmania donovani*, a KC-tropic intracellular parasite.

Conclusions: BM-derived KCs differentiate locally to resemble YS-derived KC in most but not all respects, with implications for models of infectious diseases, liver injury and bone marrow transplantation. In addition, the gene signature we describe

adds to the tools available for distinguishing KC subpopulations based on their ontology.

Keywords: Kupffer cells, liver macrophages, *Listeria, Neisseria, Salmonella, Leishmania*, scavenger receptors.

Introduction:

Kupffer cells (KCs), the resident tissue macrophages of the liver have a crucial role in both the pathogenesis and the resolution of various liver diseases and inflammatory states including alcohol-induced liver injury [1], non-alcoholic fatty liver disease (NAFLD) associated with obesity [2], ischemia reperfusion injury [3], immune tolerance to organ transplantation [3] and infectious disease [4].

Resident tissue macrophages, including KCs, were historically considered a hematopoietic population, with replenishment of the tissue reservoir from monocyte-derived precursors in the steady state. This view has now been challenged with the majority of tissue macrophages shown to develop independently of haematopoetic stem cells, being seeded in the tissues prior to birth from a population of yolk sac (YS) derived macrophages [5, 6]. These cells show some level of radiation resistance [7] and are independent of replenishment by monocytes in the steady state [8, 9]. Parallel studies that identified the transcription factors MafB and c-Maf as the factors that control the self-renewal of differentiated macrophages [10], and the observation that tissue macrophages are capable of self-renewal in models of acute inflammation [11] and under Th2 conditions in the presence of IL-4 [12], have confirmed that mature tissue macrophages are capable of proliferation and self-renewal. Finally, recent landmark studies have demonstrated that macrophage identity is unique to each

macrophage population and is plastic, with phenotype conferred by microenvironment rather than cellular origin [13-15]. Together, the above studies represent a paradigm shift in the field of tissue macrophage biology.

The studies described above all examined the origin of tissue macrophages only in the steady-state. However, there is clear evidence that infection or tissue injury, and the associated inflammatory response, promotes the recruitment of myeloid cells, mostly monocytes into peripheral tissues. It is unclear when, and if, the newly infiltrated monocytes undergo differentiation into macrophages in situ. In fact, some authors have described the infiltrating cells as tissue macrophages [16], sometimes as early as 24hrs post infiltration [17] without defining any phenotypic or functional changes in the cells. Although once infiltrated, monocytes begin differentiating into cells that are similar to the macrophages in the tissue that they reside in [18], the function of these bone marrow (BM)-derived monocytes once they are present in the tissue has not been fully investigated. Given that KCs are implicated in the pathogenesis and the resolution of a number of liver diseases [2-4, 19-21] and their phagocytic capacity makes them an easy target for particle based therapeutics [22], a greater understanding of KC biology and heterogeneity will facilitate the development of targeted liver therapeutics. Understanding whether distinct functions can be attributed to KCs of different origin will also be important for the design of new anti-infective strategies.

Here, we have used an irradiation bone marrow chimera model to enforce loss of YS-derived KCs and repopulation of the KC niche from BM-derived precursors. Using intravital microscopy to characterize the morphological and dynamic properties of

YS- and BM-derived KCs in situ, and microarray analysis to examine gene expression profile, we show that after 6 weeks of differentiation in the liver, BM-derived "KCs" closely resemble but are not fully identical to the YS-derived KCs they have replaced. Whilst uptake of acetylated low density lipoprotein (Ac-LDL) was more prominent in YS-derived macrophages and the converse was true for bacterial uptake, for most of the functional studies we performed, these populations were functionally similar. This was particularly notable in their capacity to exert early control of and direct granuloma formation in response to infection with the KC-tropic intracellular protozoan parasite *Leishmania donovani*. These findings demonstrate that in the context of enforced liver inflammation, bone marrow derived monocytes transition into KCs, which are as capable of protecting the host from infectious challenge as their YS-derived counterparts.

Materials and Methods:

For detailed methods see supplementary materials.

Ethics Statement:

All experiments were approved by the University of York Animal Welfare and Ethical Review Body and performed under UK Home Office license ('Immunity and Immunopathology of Leishmaniasis' Ref # PPL 60/3708) or approved by the QIMRB animal ethics committee Ref #P2076 (A1412-614).

Intravital imaging

Mice were anaethetised and surgery performed similar to previously described [23] except that anaethesia was maintained by inhalation of 4% isofluorane (Abbott

laboratories, UK). Images were acquired on an inverted LSM 780 multiphoton microscope (Carl Zeiss Microimaging), maintained at 36^{o}C by a blacked-out environmental chamber (Solent Scientific, UK). Images were acquired with a 40x 1.1 water immersion objective and fluorescence excitation provided by a Chameleon XR Ti:sapphire laser (Coherent) tuned to 870nm.

Whole Genome Array

RNA was isolated from purified KC and amplified via Agilent low-input Quick Amp labelling kit (Agilent Technologies). Amplified RNA was then assayed with Agilent SurePrint G3 mouse GE 8x60k microarray chips that were scanned with an Agilent C Scanner with Surescan High Resolution Technology (Agilent Technologies). The data were normalized using the percentile shift method to the 75th percentile. Comparison of the gene expression data between liver resident and BM-derived KCs was performed using the Benjamini and Hochberg false discovery rate (FDR) correction [24]. This analysis was performed with GeneSpring software (version 9; Agilent) as a standard 5% FDR, with the variances assessed by the software for each t test performed. A 2-fold expression criteria was then applied to each gene list. Gene ontology analysis was performed using the GeneSpring (Agilent) and Ingenuity pathway systems analysis software packages (Ingenuity Systems). Gene expression data is available from EBI Array Express (Accession number to be included on publication).

Results:

Radiation-induced Liver Injury Causes Loss of a Proportion of Liver Resident KCs and their Replenishment from the Bone Marrow.

To study KCs, we used (LysM-Cre x mT/mG)$_{F1}$ mice. To confirm that the majority of KCs expressed cre and were therefore GFP$^+$ in this system, we performed immunofluorescent staining on fixed liver tissue. By this assay, 95% ± 2.04% of F4/80$^+$ KCs expressed GFP. We therefore used these mice in subsequent experiments. We generated BM chimeras by irradiating (LysM-Cre x mT/mG)$_{F1}$ mice and reconstituting them with wild type C57BL/6 BM (**Figure 1A**). This process resulted in transient liver damage and inflammation as assessed by a small but non-significant increase in alanine aminotransferase (ALT) and aspartate transaminase (AST) levels in the serum of irradiated mice compared to control, non-irradiated mice (Figure 1B and C). Histological examination of H&E sections revealed detectable portal and lobular inflammation at 24hrs (Figure 1E) and 3 days post-irradiation in one out of 3 mice in each group (Figure 1F), but this was no longer visible after 7 days (Figure 1G).

A proportion of the YS-derived macrophages that express GFP were lost as a result of irradiation, and these cells were replaced by F4/80$^+$ GFP$^-$ BM-derived KCs in the chimeric mice at 6 weeks post-irradiation (**Figure 1H**). Conversely, reciprocal (LysM-Cre x mT/mG)$_{F1}$ → C57BL/6 chimeras resulted in a loss of a proportion of GFP$^-$ YS-derived KCs and their replacement with BM-derived GFP$^+$ F4/80$^+$ KCs at 6 weeks post-irradiation (**Figure 1H**). Flow cytometric analysis of digested livers (**Figure 1I)** with gating on CRIg$^+$ F4/80^{hi} cells (**Figure 1I**) demonstrated that both GFP$^+$ and GFP$^-$ KCs were present in chimeric mice. Importantly, the generation of mixed BM chimeras in this way allows for analysis of the function of each population in situ under the same microenvironmental conditions.

We then studied the kinetics of KC depletion and repopulation after irradiation in (LysM-Cre x mT/mG)$_{F1}$ → C57BL/6 chimeras. The percentage of GFP$^+$ cells that express CRIg and F4/80 and the total number of CRIg$^+$ F4/80$^+$ GFP$^+$ cells (**Figure 1J**) increased over time after irradiation to reach approximately 50% of the KC population by 6 weeks post-irradiation. We next used 2-photon real-time *in vivo* imaging of these reciprocal chimeras (**Figure 1K and L**) to examine the morphology and motility of each KC population in situ. In C57BL/6 → (LysM-Cre x mT/mG)$_{F1}$ chimeras, GFP$^+$ YS-derived KCs were large, interdigitating cells that were active in their membrane movements, but did not travel along the sinusoids (**Figure 1L and Supplementary movie 1**). BM-derived KCs observed in (LysM-Cre x mT/mG)$_{F1}$ → C57BL/6 chimeras also showed similar morphology and remained stationary within the sinusoids, confirming that they had become resident within the liver (**Figure 1L and Supplementary movie 2**). Analysis of KC volume and surface area demonstrated that YS-derived KCs were somewhat larger than BM derived KCs (**Figure 1K**). Taken together, these data demonstrate that following genotoxic damage BM-derived cells differentiate morphologically into KCs and become resident in the liver.

An Ion Homeostasis Gene Signature Distinguishes Tissue-Resident from BM-derived KCs.

We next sought to determine whether BM-derived KCs had indeed acquired global characteristics of YS-derived KCs via a comparative gene expression approach. BM-derived and YS-derived KCs were isolated from chimeric mice by fluorescence activated high speed cell sorting according to size, granularity and expression of CRIg

(**Figure 2A**). KCs were then further separated into GFP^+ and GFP^- cell fractions. Sorted populations were typically >90% pure for the population of interest. Giemsa stained cytopsin preparations of sorted cells demonstrated that BM-derived and YS-derived KCs had similar macrophage-like morphology (**Figure 2B**). Gene expression analysis by microarray demonstrated that of the annotated genes that were represented on the chips, BM-derived and YS-derived KCs shared expression of >99% of the probes, with only 42 probes meeting criteria for differentially binding of the cDNA between the two populations (5% FDR with 2 fold cut-off, **Table 1, Figure 2C**). Of note, the binding of these 42 transcripts was present for the resident KC population and lacking in BM-derived KCs. There were no transcripts uniquely present in BM-derived KCs. KCs showed similar transcript profiles whether isolated from chimeras that resulted in them being GFP^+ or GFP^-, with no significant differences in expression observed within the GFP^+ and GFP^- fractions within the same KC population (data not shown).

Validation of differential expression of a proportion of the genes listed in Table 1 was then performed by measuring mRNA abundance by real time PCR, using RNA isolated from independently sorted samples of each KC population. mRNA abundance for *Cd163*, *Marco*, *Ric3*, *Colec12* and *Timd4* (**Figure 2D**) was higher in YS-derived KCs than in BM-derived KCs, confirming the microarray data (**Figure 2C**). Abundance of *Clec4f* mRNA was similar between the populations, also confirming the microarray data and validating that a transition to KC, as defined by *Clec4f* (Kupffer Cell Receptor), had occurred in the BM-derived KC population.

Macrophage Receptor with Collagenous Structure (MARCO) was one of the most differentially expressed genes found in YS-derived KCs, with 15-fold higher mRNA abundance than seen in BM-derived KCs. We therefore analysed the expression of MARCO protein in KCs in C57BL/6 → (LysM-Cre x mT/mG)$_{F1}$ chimeras. Clear co-expression of MARCO and GFP was observed in YS-derived KCs, but very little detectable expression of MARCO in GFP$^-$ BM derived KCs (**Figure 2E**). In further validation experiments, flow cytometry on isolated hepatic mononuclear cells from B6.MacGreen → C57BL/6 chimeras demonstrated that Tim4 was expressed in 73.4 +/- 4.21% of YS-derived KCs and only expressed in 5 +/- 0.26% of BM-derived KCs confirming that Tim4 expression is enriched within the YS-derived KC population.

To gain a better understanding of the implications of the transcriptomic differences between YS-derived and BM-derived KCs, we performed gene ontology (GO) analysis. 3 of the 4 gene ontology terms that showed highly significant enrichment ($P<0.001$) were associated with ion homeostasis (Supplementary **Table 1**). This included GO:0055065; metal ion homeostasis, GO:0055080; cation homeostasis and GO:0050801; ion homeostasis. This enrichment was associated specifically with the expression of *Ric3*, *Ank2*, *Slc22a17*, *Epor* and *Hmox1* in YS-derived KCs (**Figure 2C**). Resistant to inhibitors of cholinesterase 3 (Ric3) is a transmembrane protein that controls expression of nicotinic acetylcholine receptors, which are gated ion channels [25]. Ankyrin 2 (Ank2) is also associated with ion channels, being an adaptor protein for connection of ion channels to the actin cytoskeleton [26]. Slc22a17 (also known as 24p3R) is associated with iron uptake and apoptosis [27]. In addition, mRNA for the erythropoietin receptor (*Epor*), hemeoxygenase 1 (*Hmox1*), both associated with red

blood cell homeostasis and the hemoglobin scavenger receptor *Cd163* [28] were more abundant in YS-derived KCs, the latter being one of the most differentially expressed genes (**Figure 2C**).

BM-derived and YS-derived KCs exhibit comparable clearance of effete RBCs

We next set out to determine if both KC populations were comparable in a range of functional assays. First we studied another essential function of KCs, namely the clearance of effete RBCs. We injected neuraminidase-treated PHK-26-labelled RBCs [29] intravenously into chimeric mice and assessed their uptake by BM-derived or YS-derived KC populations by flow cytometry. These data showed that at 2 weeks post-irradiation, although still at low frequencies in the liver (**Figure 1**), differentiated BM-derived KCs were capable of phagocytosing RBCs with the same efficiency as their YS-derived counterparts (**Figure 3A**). A similar pattern was observed at 6 weeks post-irradiation (**Figure 3B**). Hence, differentiation to allow for this essential KC function occurs rapidly once BM-derived cells enter the liver microenvironment.

YS-Derived Macrophages more efficiently accumulate acetylated Low Density Lipoproteins (LDL).

Given that YS-derived macrophages had a scavenger phenotype, we next utilised the BM chimera model to examine the uptake of acetylated low density lipoprotein (Ac-LDL) by BM- and YS-derived liver macrophages. Hepatic mononuclear cells from BM chimeric mice were isolated and incubated with fluorescently labelled Ac-LDL. The proportion of YS-derived macrophages that were positive for LDL accumulation

was significantly higher than that for BM-derived macrophages (Fig 3C), consistent with the differential expression of scavenger receptors in these two populations.

In vivo Response of KC to LPS challenge

KCs play a major role in the innate immune response to infection and are continually conditioned by endotoxin draining from the intestinal tract [30-32]. Previous *in vitro* studies have demonstrated that multiple exposure to LPS may lead to a state of LPS tolerance, wherein a second exposure to LPS fails to induce gene expression to a similar extent as the primary exposure [33]. Furthermore, Medzhitov and colleagues have argued that LPS inducible genes can be classified as "tolerizable" or non-tolerizable", reflecting different epigenetic regulation of transcription [34]. It might be expected that KCs had mechanisms to avoid loss of function due to LPS tolerance and that this might represent one aspect of tissue specific conditioning [15]. We therefore asked whether genes that were not expressed by BM-derived KCs in the steady state were LPS inducible. We treated bone marrow chimeric mice with LPS, sorted the BM-derived and YS-derived KCs 24 hours later and used real-time PCR to analyze mRNA abundance for a selected panel of genes. *Marco* is an example of a non-tolerizable gene and is expressed exclusively in YS-derived KCs (**Figure 4A**). LPS treatment had no effect on *Marco* mRNA levels in either YS-derived or BM-derived KCs (**Figure 4A**) suggesting that the differences observed in baseline levels of MARCO mRNA were not a result of differences in long term LPS exposure between the two populations. LPS treatment resulted in a down-regulation of *Cd163* mRNA abundance in YS-derived KCs, but had no effect on the minimal abundance of *Cd163* mRNA in BM-derived KCs (**Figure 4B**). Similarly, LPS treatment reduced

the abundance of *Ric3* and *Timd4* mRNA in YS-derived KCs and decreased *Clec4f* mRNA abundance in both populations of KCs (**Figure 4C-E**). These data indicate that even high dose LPS exposure does not drive the final differentiation of BM-derived KCs to match the gene expression profile of YS-derived KCs, at least for the genes assayed here, and it appears that both populations are capable of responding to LPS challenge.

YS-derived and BM-derived KCs show differential uptake of bacteria pathogens

Given that KCs are central to the clearance of systemic bacteria and MARCO has been associated with bacterial uptake [35-37], we next assessed the ability of YS- and BM-derived macrophages to take up three different bacterial pathogens. For these experiments, we generated B6.MacGreen → B6.CD45.1 BM chimeras and injected fluorescently labelled, heat-killed *Salmonella enterica* subspecies *enterica* serovar Typhimurium (*S*. typhimurium), *Neisseria meningitidis* or *Listeria monocytogenes*. Phagocytosis was assessed 2 hours after intravenous injection of bacteria by flow cytometry on isolated hepatic MNCs or by fluorescence microscopy on whole liver tissue (Figure 5). Unexpectedly, our data showed that a greater proportion of BM-derived KCs phagocytosed *N. meningitidis* and *L. monocytogenes*, compared to YS-derived KC, with a similar trend also observed for *S. typhimurium* (Figure 5E). Collectively with our data above on erythrophagocytosis, we conclude that whilst phagocytosis per se is not a unique property of either KC population, differences in phagocytic clearance rate based on ligand specificity exist.

YS-derived and BM-derived KCs respond similarly to *Leishmania* infection.

Finally, we evaluated the ability of these two KC populations to respond to and contain infectious challenge by a KC-tropic intracellular parasite. *Leishmania donovani* infection of mice via the intravenous route leads to rapid KC infection and the subsequent T cell-dependent generation of inflammatory foci termed granulomas [23, 38, 39]. We infected reciprocal BM chimeric mice with transgenic tdTomato-expressing *L. donovani* amastigotes, and determined the proportion of KCs of each origin that were infected. Unlike the situation observed with bacterial uptake (Figure 5), YS-derived and BM-derived KCs did not differ in their ability to phagocytose *L. donovani,* (**Figure 6A**). Both populations were capable of killing parasites, as judged by a decrease in the percentage of infected cells observed by 48hrs post-injection (**Figure 6A**), though this difference only reached significance for BM-derived KCs. The difference between BM-derived and YS-derived KCs at 48hrs post-infection was not significant (**Figure 6A**) suggesting that both populations are capable of controlling infection with *L. donovani*. By 7 days post-infection, both KC populations showed a reduction in percentage of infected cells when compared to the 2hr time point (**Figure 6A**), indicating a similar level of control of infection.

Furthermore, quantifying the number of parasites within each infected KC showed that BM-derived and YS-derived KCs phagocytosed the same number of parasites at 2hrs post-injection and had equal numbers of parasites per cell by 7 days post-infection (**Figure 6B**). These data, in conjunction with those shown in Figure 6A suggest that those KCs that do not clear infection are able to similarly support parasite

multiplication and an increase in the mean number of parasites present per cell (**Figure 6B**).

As an additional measure of function, we examined the ability of these two populations of KCs to become the focus for granuloma formation. Inflammatory foci were scored into 5 categories: foci that contained only YS-derived KCs, mostly YS-derived KCs a 50:50 mix of YS- and BM-derived KCs, mostly BM-derived KCs and only BM- derived KCs. By this analysis, we were able to show that inflammatory foci were more likely to be formed around BM-derived KCs than around YS-derived KCs (**Figure 5C**)**,** although both KC populations were capable of seeding granuloma formation. Examples of granulomas from YS-derived KCs (**Figure 5D**), BM-derived KCs (**Figure 5E**) and mixed granulomas (**Figure 5F**), were evident in all infected mice.

In summary, our data collectively argue that BM-derived KC are not only capable of differentiating in the liver to look and act like YS-derived KCs but are also capable of responding to an infectious challenge in a similar way.

Discussion:

The recent investigations into the origins of tissue macrophages in mice have demonstrated that in the lung, spleen, skin, pancreas, kidney and liver, tissue resident macrophages are not derived from haematopoeitic precursors in the steady state, but are seeded in embryonic tissues (YS-derived) and self-maintain locally in adult tissues

[5, 8, 9]. We have now shown that following irradiation induced liver damage, YS-derived KCs are partially replaced by BM-derived precursors, and that these cells differentiate in the liver into mature KCs, where they become resident and share >99% of their gene expression with YS-derived KCs. Although functionally distinct regarding Ac-LDL uptake (YS>BM) and phagocytosis of bacteria (BM>YS), these newly differentiated, BM-derived KCs are equally capable of responding to soluble (LPS) and parasitic insult as YS-derived KCs and to equally perform essential housekeeping functions like RBC clearance. We have also identified a combination of phenotypic markers including Marco and Tim4 that along with well characterised molecules including CRIg and F4/80 can be used to phenotypically separate liver macrophages that are recently BM-derived or of YS-origin.

The recent investigations and characterisation of Clec4f through gene knockout and sequencing approaches [15, 40] have confirmed Clec4f as a KC-restricted molecule, making it a good candidate molecule for defining KC differentiation. These investigations have now been further expanded by Scott et al to include specific depletion of KC in the liver through the use of KC-DTR mice in which the human DTR gene was inserted into the 3' untranslated region of the *Clec4f* gene. Administration of DT resulted in specific depletion of KCs in the liver [18]. We found that BM-derived KCs up regulate *Clec4f* gene expression and take up their characteristic stationary sinusoidal position, becoming KCs by all morphologic and dynamic definitions that are currently available. In their recent study, Lavin et al described steady state (and presumably mostly YS-derived) KC as most closely associated with red pulp macrophages of the spleen, in terms of gene expression in these two populations. It is noteworthy, therefore, that YS-derived KCs, but not BM-

derived KCs in our study have abundant mRNA for *Ric3*, *CD163*, *St6galnac2*, *Epor*, *Hmox1* and *Ecm1,* genes also reported in the ImmGen database as highly expressed in red pulp macrophages. These data suggest that full acquisition of housekeeping properties conserved between splenic and YS-derived KCs has not yet occurred in the BM-derived KCs we have studied.

Whilst this manuscript was under review, Scott et al published gene signatures distinguishing YS-derived KCs from BM-derived KCs obtained at different times post DTR-mediated depletion of YS-derived KCs [18]. Their data show many similarities, but some differences with that presented here. Of note, however, five (*Timd4*, *Colec12*, *Cd163*, *Snrpn* and *Xlr*) of the twelve genes described as differentially expressed in YS but not BM-derived KCs in their study [18] were also identified by us, providing confidence in their assigment independent of methodology used.

In addition to the 5 commonly identified genes associated with YS-derived KCs, we also idenitifed a further 37 transcripts that were differentially expressed. Analysis of these showed enrichment in YS-derived KCs for GO terms related to ion homeostasis, and differential expression of genes associated with red blood cell phagocytosis and turn-over. However, our data using an *in vivo* phagocytosis assay demonstrated no difference in the ability of BM-derived and YS-derived KCs to phagocytose labelled red blood cells, suggesting that the two populations were equally capable of contributing to this important KC function [41]. Nevertheless, further studies will be required to determine whether differences exist between the two populations in the scavenging of haemoglobin and the break down and recycling of red blood cells.

It was of significant note that there were no genes expressed by BM-derived cells that were not expressed by YS-derived KCs. This is in contrast to the findings of Scott et al who found two genes (*Ccr3 and Tspan32*) that were uniquely expressed by bone marrow-derived KCs [18]. Together, the similarity in gene expression profiles in these two studies suggest that BM-derived monocytes are malleable in nature and responsive to the microenvironmental cues they receive, enabling them to differentiate and perform functions required by the tissue that they become resident in. It would follow that this is not hindered by extensive residual expression of a BM-specific gene signature that cannot be reprogrammed when required.

These studies confirm and further extend the observations of others, that irradiation induces a loss of a proportion of YS-derived macrophages in a number of tissues [7, 8, 42], triggering repopulation from BM-derived precursors. In non-radiation induced depletion models, loss of a proportion of the tissue resident macrophage population, induces local proliferation and repopulation by self-renewal in the lungs, liver, epidermis and brain [5]. In contrast, the depletion of tissue-derived macrophages via irradiation appears to trigger a different mechanism of repopulation, with long-term seeding of hematopoietic stem cell-derived cells being a predominant feature of repopulation in the spleen, lungs, peritoneum and bone marrow[8]. This difference is likely associated with the absence (conditional gene targeting) vs presence (irradiation) of collateral damage and the induction of stress induced responses in a multitude of different cell types in any given organ. However in the liver, complete loss of KCs via clodronate liposome mediated depletion also results in repopulation of

KCs from BM precursors [7], implying that there may be a threshold that triggers differentiation of BM-derived cells when the niche cannot be sufficiently filled by the proliferation of the YS-derived population. This phenomenon may be a secondary safety net for the function of the liver, as the BM-derived KCs appear to be capable of differentiating in situ to have a very similar gene expression profile to the cells they replace, with a similar ability to respond to an infectious challenge.

The use of the BM chimera model allowed us to evaluate the functional capacity of YS- and BM-derived KCs in a uniform microenvironment, obviating any differences in global liver function that might otherwise have arisen if we had used a total replacement strategy [18]. Uptake of *E.coli* in vitro by isolated YS- and BM-derived KCs has been reported to be similar [18]. In contrast, to study KC function we used an extended battery of in vivo assays that retain natural micoenvironmental context and that employed both soluble and particulate ligands. In addition, we used a well-characterised parasitic model that allowed us to monitor innate microbicidal activity as well as T cell dependent host protective immunity (expressed as granulomatous inflammation). Whereas uptake of Ac-LDL was more efficient in YS-derived KCs, we found that BM-derived KCs were more phagocytic towards *L. monocytogenes*, *N. meningitides* and *S. typhimurium.* As MARCO has been implicated in uptake of each of these bacteria, this result was unexpected. The differences were not absolute, but may suggest that with increasing ligand complexity, there is greater scope for receptor redundancy and / or cooperativity, a level of complexity that is not fully captured by gene expression analysis. For example, both *N. meningitides* and *L. monocytogenes* utilize SR-A in addition to MARCO to interact with macrophages [35], a molecule

that showed no difference in expression between the two macrophage populations at an RNA level in our gene expression studies.

Our data are not without clinical relevance, where radiation-induced liver damage (radiation hepatitis) can result in hepatic fibrosis. Bone marrow transplantation for treatment of haematological malignancy uses total body irradiation (TBI) as a pre-conditioning strategy prior to transplantation. In this system, the remaining host macrophages [43] including KCs in the liver [44] have been implicated in the suppression of the pathological graft versus host disease (GVHD) response. Whether a similar level of radiation resistance is observed in human Kupffer cells requires further investigation. Given that inflammatory events and the resultant cellular turnover are likely common in the liver in vivo, it is essential that BM-derived KCs have host protective functions as well as functional competence to maintain the homeostatic functions of the liver. In spite of some selected functional differences, our data provide strong evidence that this is indeed the case.

Acknowledgements:

All microarray data are deposited in EBI Array Express (accession number E-MTAB-4954). We wish to thank the staff of the Biological Services Facility and P. O'Toole, K. Hodgkinson, K. Hogg, G. Park, J. Marrison, and C. Whalley (Technology Facility, Department of Biology, University of York) for technical assistance. We wish to thank Genentech Inc for supplying the anit-CRIg antibody. We wish to thank Dr Cheryl-Lynn Ong, Dr Jayde Gawthorne, Saiyuri Naicker, Dr Nick West, and Professor Alastair McEwan (School of Chemistry and Molecular Biosciences, University of Queensland) for the

supply of the heat killed bacterial strains. Thank you to Professor Andrew Clouston (Envoi Pathology, and the University of Queensland) for scoring pathology in the liver post-irradiation. This work was supported by the UK Medical Research Council (Grant #G0802620) and the Australian National Health and Medical Research Council (Grant #APP1105817).

Figure Legends

Figure 1: Characterisation of YS- and BM-derived KCs. **A)** Experimental approach used to generate irradiation chimeras with GFP$^+$ YS-derived KCs. **B)** ALT and **C)** AST levels in the serum of mice at different time points post-irradiation as compared to control (non-irradiated) animals. D) H&E stained sections from the liver of control non-irradiated mice or mice E) 24hrs F) 3 days or G) 7 days post-irradiation demonstrating very little liver damage or inflammation as a result of irradiation. H) Immunofluorescent image demonstrating the presence of GFP$^+$ F4/80$^+$ liver resident KCs and GFP$^-$ F4/80$^+$ BM-derived KC in the livers of the chimeras generated in A) (left) or reciprocal chimeras (right), 6 weeks post-irradiation. GFP (green), F4/80 (red). **I)** Flow cytometry analysis of the livers of chimeras generated via the method shown in A) gated on FSC and SSC, CRIg and F4/80 expression and GFP. **J)** Analysis of the percentage of CRIg$^+$ F4/80$^+$ cells that express GFP (left) and the number of CRIg$^+$ F4/80$^+$ GFP$^+$ cells in the liver (right) over time. Symbols represent individual mice and are representative of 2 experiments with 5-6 mice per group. **I)** The volume and surface area of KCs in 3 dimensions. L) 2-photon intravital imaging of YS-derived KCs in the livers of chimeras generated via the method shown in (A) (top) or the reciprocal chimera (bottom). Data were analysed with a non-parametric t test. * <0.05.

Figure 2: Transcriptional analysis of YS- and BM-derived KCs. **A)** Isolation of YS-derived and BM-derived KCs by high-speed fluorescence activated cell sorting according to forward and side scatter, GFP and CRIg. Post-sort purity of GFP^+ and GFP^- KCs. **B)** Giemsa stained cytospins of sorted BM derived (left) or liver resident (right) KCs. **C)** Heat maps demonstrating the differential binding to probe sets across the biological replicates for selected groups of genes. **D)** Accumulation of mRNA for selected genes expressed as relative expression to HPRT. Individual symbols are representative of KCs sorted from individual mice. Data were analysed using a non-parametric t test. ** P< 0.01. **E)** Immunofluorescent images demonstrating the expression of MARCO (white) on GFP^+ (green) $F4/80^+$ (red) liver resident KCs at 200x (top) and 630x (bottom) magnification.

Figure 3: YS and BM-derived KCs have similar capacity to clear neuraminidase treated labelled red blood cells. C57BL/6 recipient mice received B6.mTmG.LysM^{Cre} bone marrow and PKH26 labelled red blood cells **A)** two weeks or **B)** 6 weeks post-irradiation. Hepatic mononuclear cells were prepared and plots gated on $CRIg^+$ and GFP expression to examine four populations. $CRIg^-GFP^+$ BM-derived cells. $CRIg^+GFP^+$ differentiated BM- derived KCs. $CRIg^+GFP^-$ YS-derived KCs and $CRIg^-GFP^-$ non-macrophage liver resident cells. The $PKH26^+$ proportion of each population is shown. Data are representative of two independent experiments with at least 4 mice/group. **C)** Uptake of acetylated LDL as assessed by flow cytometry within $F4/80^{hi}$ $CD11b^{lo}$ GFP^+ BM- or GFP^- YS derived KCs expressed as a percentage of each population.

Figure 4: LPS responsiveness of YS- and BM-derived KCs**.** CD45.1/.2 chimeras that were 6 weeks post-irradiation were treated with 100μg of LPS or sham treated and the KCs isolated 24 hours later. Groups of 8 chimeric mice were treated and 2 livers pooled to make 4 individual replicates per treatment group. KCs were sorted into YS- and BM-

derived populations based on expression of CD45.1, F4/80, and CRIg. **A)** Relative expression of *CD163*, **B)** *Marco*, **C)** *Ric3*, **D)** *Timd4* and **E)** *Clec4f*. Data are pooled from 2 separate experiments. Data were tested for normal distribution and then analysed using a one-way ANOVA with post-test. **** P< 0.0001, *** P<0.001, ** P<0.01, *P<0.05.

Figure 5: Uptake of bacterial species by BM- and YS-derived KCs. Two-photon imaging of live liver tissue from B6.MacGreen → CD45.1 chimeras from **A)** control mice or mice that were injected with heat-killed, Syto 62 labelled **B)** *S. typhimurium*, **C)** *Neisseria meningitidis* or **D)** *Listeria monocytogenes*. **E)** Quantification of bacterial uptake by $F4/80^{hi}$ $CD11b^{lo}$ GFP^{+} BM- or GFP^{-} YS-derived KCs by flow cytometry.

Figure 6: Control of *Leishmania* infection by YS- and BM-derived KCs. **A)** Percentage of liver BM derived (white bars) and liver resident (grey bars) KCs that are infected at 2hrs, 48hrs and 7 days post-infection with *L. donovani*. **B)** The number of parasites per cell in BM derived (white bars) and liver resident KCs (grey bars). **C)** The percentage of inflammatory foci formed at 7 days post-infection that are made up of resident or BM derived KCs. Data were analysed via Kruskal-Wallis test. * P<0.05, ***P<0.001. **D)** Immunofluorescent images demonstrating an inflammatory focus predominantly made up of liver resident KCs (green). F4/80 (red), *L. donovani* (white). **E)** Immunofluorescent images demonstrating an inflammatory focus predominantly made up of BM derived KCs (green). F4/80 (red), *L. donovani* (white). **F)** Immunofluorescent images demonstrating an inflammatory focus made up of a mixture of liver resident (green) and BM derived KCs (red). F4/80 (red), *L. donovani* (white).

[1] Ajakaiye M, Jacob A, Wu R, Nicastro JM, Coppa GF, Wang P. Alcohol and hepatocyte-Kupffer cell interaction (review). Molecular medicine reports 2011;4:597-602.
[2] Baffy G. Kupffer cells in non-alcoholic fatty liver disease: the emerging view. Journal of hepatology 2009;51:212-223.
[3] Huang HF, Zeng Z, Chen MQ. Roles of Kupffer cells in liver transplantation. Hepato-gastroenterology 2012;59:1251-1257.
[4] Protzer U, Maini MK, Knolle PA. Living in the liver: hepatic infections. Nature reviews Immunology 2012;12:201-213.
[5] Schulz C, Gomez Perdiguero E, Chorro L, Szabo-Rogers H, Cagnard N, Kierdorf K, et al. A lineage of myeloid cells independent of Myb and hematopoietic stem cells. Science 2012;336:86-90.
[6] Ginhoux F, Greter M, Leboeuf M, Nandi S, See P, Gokhan S, et al. Fate mapping analysis reveals that adult microglia derive from primitive macrophages. Science 2010;330:841-845.
[7] Klein I, Cornejo JC, Polakos NK, John B, Wuensch SA, Topham DJ, et al. Kupffer cell heterogeneity: functional properties of bone marrow derived and sessile hepatic macrophages. Blood 2007;110:4077-4085.
[8] Hashimoto D, Chow A, Noizat C, Teo P, Beasley MB, Leboeuf M, et al. Tissue-Resident Macrophages Self-Maintain Locally throughout Adult Life with Minimal Contribution from Circulating Monocytes. Immunity 2013;38:792-804.
[9] Yona S, Kim KW, Wolf Y, Mildner A, Varol D, Breker M, et al. Fate Mapping Reveals Origins and Dynamics of Monocytes and Tissue Macrophages under Homeostasis. Immunity 2012.
[10] Aziz A, Soucie E, Sarrazin S, Sieweke MH. MafB/c-Maf deficiency enables self-renewal of differentiated functional macrophages. Science 2009;326:867-871.
[11] Davies LC, Rosas M, Smith PJ, Fraser DJ, Jones SA, Taylor PR. A quantifiable proliferative burst of tissue macrophages restores homeostatic macrophage populations after acute inflammation. European journal of immunology 2011;41:2155-2164.
[12] Jenkins SJ, Ruckerl D, Cook PC, Jones LH, Finkelman FD, van Rooijen N, et al. Local macrophage proliferation, rather than recruitment from the blood, is a signature of TH2 inflammation. Science 2011;332:1284-1288.
[13] Okabe Y, Medzhitov R. Tissue-specific signals control reversible program of localization and functional polarization of macrophages. Cell 2014;157:832-844.
[14] Gosselin D, Link VM, Romanoski CE, Fonseca GJ, Eichenfield DZ, Spann NJ, et al. Environment drives selection and function of enhancers controlling tissue-specific macrophage identities. Cell 2014;159:1327-1340.
[15] Lavin Y, Winter D, Blecher-Gonen R, David E, Keren-Shaul H, Merad M, et al. Tissue-resident macrophage enhancer landscapes are shaped by the local microenvironment. Cell 2014;159:1312-1326.
[16] Karlmark KR, Zimmermann HW, Roderburg C, Gassler N, Wasmuth HE, Luedde T, et al. The fractalkine receptor CX(3)CR1 protects against liver fibrosis by controlling differentiation and survival of infiltrating hepatic monocytes. Hepatology 2010;52:1769-1782.
[17] Karlmark KR, Weiskirchen R, Zimmermann HW, Gassler N, Ginhoux F, Weber C, et al. Hepatic recruitment of the inflammatory Gr1+ monocyte subset upon liver injury promotes hepatic fibrosis. Hepatology 2009;50:261-274.
[18] Scott CL, Zheng F, De Baetselier P, Martens L, Saeys Y, De Prijck S, et al. Bone marrow-derived monocytes give rise to self-renewing and fully differentiated Kupffer cells. Nat Commun 2016;7:10321.
[19] Ajakaiye M, Jacob A, Wu R, Nicastro JM, Coppa GF, Wang P. Alcohol and hepatocyte-Kupffer cell interaction (review). Mol Med Rep 2011;4:597-602.

[20] Enomoto N, Ikejima K, Bradford BU, Rivera CA, Kono H, Goto M, et al. Role of Kupffer cells and gut-derived endotoxins in alcoholic liver injury. Journal of gastroenterology and hepatology 2000;15 Suppl:D20-25.
[21] Enomoto N, Ikejima K, Kitamura T, Oide H, Takei Y, Sato N, et al. Alcohol enhances lipopolysaccharide-induced increases in nitric oxide production by Kupffer cells via mechanisms dependent on endotoxin. Alcoholism, clinical and experimental research 2000;24:55S-58S.
[22] Tacke F, Zimmermann HW. Macrophage heterogeneity in liver injury and fibrosis. Journal of hepatology 2014.
[23] Beattie L, Peltan A, Maroof A, Kirby A, Brown N, Coles M, et al. Dynamic imaging of experimental Leishmania donovani-induced hepatic granulomas detects Kupffer cell-restricted antigen presentation to antigen-specific CD8 T cells. PLoS pathogens 2010;6:e1000805.
[24] Pawitan Y, Michiels S, Koscielny S, Gusnanto A, Ploner A. False discovery rate, sensitivity and sample size for microarray studies. Bioinformatics 2005;21:3017-3024.
[25] Alexander JK, Sagher D, Krivoshein AV, Criado M, Jefford G, Green WN. Ric-3 promotes alpha7 nicotinic receptor assembly and trafficking through the ER subcompartment of dendrites. The Journal of neuroscience : the official journal of the Society for Neuroscience 2010;30:10112-10126.
[26] Kline CF, Scott J, Curran J, Hund TJ, Mohler PJ. Ankyrin-B regulates Cav2.1 and Cav2.2 channel expression and targeting. The Journal of biological chemistry 2014;289:5285-5295.
[27] Devireddy LR, Gazin C, Zhu X, Green MR. A cell-surface receptor for lipocalin 24p3 selectively mediates apoptosis and iron uptake. Cell 2005;123:1293-1305.
[28] Etzerodt A, Kjolby M, Nielsen MJ, Maniecki M, Svendsen P, Moestrup SK. Plasma clearance of hemoglobin and haptoglobin in mice and effect of CD163 gene targeting disruption. Antioxidants & redox signaling 2013;18:2254-2263.
[29] Bratosin D, Estaquier J, Ameisen JC, Aminoff D, Montreuil J. Flow cytometric approach to the study of erythrophagocytosis: evidence for an alternative immunoglobulin-independent pathway in agammaglobulinemic mice. Journal of immunological methods 2002;265:133-143.
[30] Benten D, Schulze zur Wiesch J, Sydow K, Koops A, Buggisch P, Boger RH, et al. The transhepatic endotoxin gradient is present despite liver cirrhosis and is attenuated after transjugular portosystemic shunt (TIPS). BMC gastroenterology 2011;11:107.
[31] Catala M, Anton A, Portoles MT. Characterization of the simultaneous binding of Escherichia coli endotoxin to Kupffer and endothelial liver cells by flow cytometry. Cytometry 1999;36:123-130.
[32] Freudenberg MA, Freudenberg N, Galanos C. Time course of cellular distribution of endotoxin in liver, lungs and kidneys of rats. British journal of experimental pathology 1982;63:56-65.
[33] West MA, Heagy W. Endotoxin tolerance: A review. Critical care medicine 2002;30:S64-S73.
[34] Foster SL, Hargreaves DC, Medzhitov R. Gene-specific control of inflammation by TLR-induced chromatin modifications. Nature 2007;447:972-978.
[35] Chen Y, Wermeling F, Sundqvist J, Jonsson AB, Tryggvason K, Pikkarainen T, et al. A regulatory role for macrophage class A scavenger receptors in TLR4-mediated LPS responses. European journal of immunology 2010;40:1451-1460.
[36] Mukhopadhyay S, Chen Y, Sankala M, Peiser L, Pikkarainen T, Kraal G, et al. MARCO, an innate activation marker of macrophages, is a class A scavenger receptor for Neisseria meningitidis. European journal of immunology 2006;36:940-949.
[37] Pluddemann A, Mukhopadhyay S, Sankala M, Savino S, Pizza M, Rappuoli R, et al. SR-A, MARCO and TLRs differentially recognise selected surface proteins from Neisseria meningitidis: an example of fine specificity in microbial ligand recognition by innate immune receptors. J Innate Immun 2009;1:153-163.

[38] McElrath MJ, Murray HW, Cohn ZA. The dynamics of granuloma formation in experimental visceral leishmaniasis. The Journal of experimental medicine 1988;167:1927-1937.
[39] Murray HW. Tissue granuloma structure-function in experimental visceral leishmaniasis. International journal of experimental pathology 2001;82:249-267.
[40] Yang CY, Chen JB, Tsai TF, Tsai YC, Tsai CY, Liang PH, et al. CLEC4F is an inducible C-type lectin in F4/80-positive cells and is involved in alpha-galactosylceramide presentation in liver. PloS one 2013;8:e65070.
[41] Terpstra V, van Berkel TJ. Scavenger receptors on liver Kupffer cells mediate the in vivo uptake of oxidatively damaged red blood cells in mice. Blood 2000;95:2157-2163.
[42] Zigmond E, Samia-Grinberg S, Pasmanik-Chor M, Brazowski E, Shibolet O, Halpern Z, et al. Infiltrating monocyte-derived macrophages and resident kupffer cells display different ontogeny and functions in acute liver injury. J Immunol 2014;193:344-353.
[43] Hashimoto D, Chow A, Greter M, Saenger Y, Kwan WH, Leboeuf M, et al. Pretransplant CSF-1 therapy expands recipient macrophages and ameliorates GVHD after allogeneic hematopoietic cell transplantation. The Journal of experimental medicine 2011;208:1069-1082.
[44] MacDonald KP, Palmer JS, Cronau S, Seppanen E, Olver S, Raffelt NC, et al. An antibody against the colony-stimulating factor 1 receptor depletes the resident subset of monocytes and tissue- and tumor-associated macrophages but does not inhibit inflammation. Blood 2010;116:3955-3963.

Table 1 – The genes differentially expressed between liver resident and BM derived KC.

Gene Symbol	Gene Name	Fold change
Cd163	CD163 antigen	26.97
Snrpn	small nuclear ribonucleoprotein N	17.82
4922501L14Rik	11 days pregnant adult female ovary and uterus cDNA, RIKEN full-length enriched library, clone:5031409G23 product:inferred:	15.47
Marco	macrophage receptor with collagenous structure	14.99
Snrpn	small nuclear ribonucleoprotein N	13.68
	lincRNA:chr7:67111261-67120697 reverse strand	12.18
Ric3	resistance to inhibitors of cholinesterase 3 homolog (C. elegans)	11.02
Colec12	collectin sub-family member 12	10.30
Timd4	T cell immunoglobulin and mucin domain containing 4	9.59
	lincRNA:chr6:36790208-36792056 reverse strand	8.72
Gm10554	PREDICTED: predicted gene 10554	8.47
Tlx1	T cell leukemia, homeobox 1	8.22
2410076I21Rik	RIKEN cDNA 2410076I21 gene	7.91
Gm5168	predicted gene 5168	6.01
Gm2030	predicted gene 2030	5.99
Mrap	melanocortin 2 receptor accessory protein	5.90
Xlr	X-linked lymphocyte-regulated complex	5.71
Slx	Sycp3 like X-linked	5.52
Speg	SPEG complex locus	5.24
	lincRNA:chr17:38132217-38157667 forward strand	4.51
Gm14625	predicted gene 14625	4.51
Hgd	homogentisate 1, 2-dioxygenase	4.48
Speg	SPEG complex locus	4.19
4933401L05Rik	adult male testis cDNA, RIKEN full-length enriched library, clone:4933401L05	4.06
Afp	alpha fetoprotein	3.92
Gm14625	predicted gene 14625	3.74
Fsd2	fibronectin type III and SPRY domain containing 2	3.69
Mcts2	Mus musculus malignant T cell amplified sequence 2	3.68
Cct6b	chaperonin containing Tcp1, subunit 6b (zeta)	3.54
	lincRNA:chr6:86477309-86537554 forward strand	3.52
Chst8	carbohydrate (N-acetylgalactosamine 4-0) sulfotransferase 8	3.50
Gm10836	adult male kidney cDNA, RIKEN full-length enriched library, clone:F530007B04	3.49
Klhl13	kelch-like 13	3.12
St6galnac2	ST6 (alpha-N-acetyl-neuraminyl-2,3-beta-galactosyl-1,3)-N-acetylgalactosaminide alpha-2,6-sialyltransferase 2	3.03
Ank2	ankyrin 2, brain	2.69
Slc22a17	solute carrier family 22 (organic cation transporter), member 17	2.58
Tnk2	tyrosine kinase, non-receptor, 2	2.49
Redrum	Redrum, erythroid developmental long intergenic non-protein coding transcript	2.42
Epor	erythropoietin receptor	2.18
Hmox1	heme oxygenase (decycling) 1	2.17
	lincRNA:chr13:62734450-62785325 forward strand	2.10
Ecm1	extracellular matrix protein 1	2.10

Figure 1

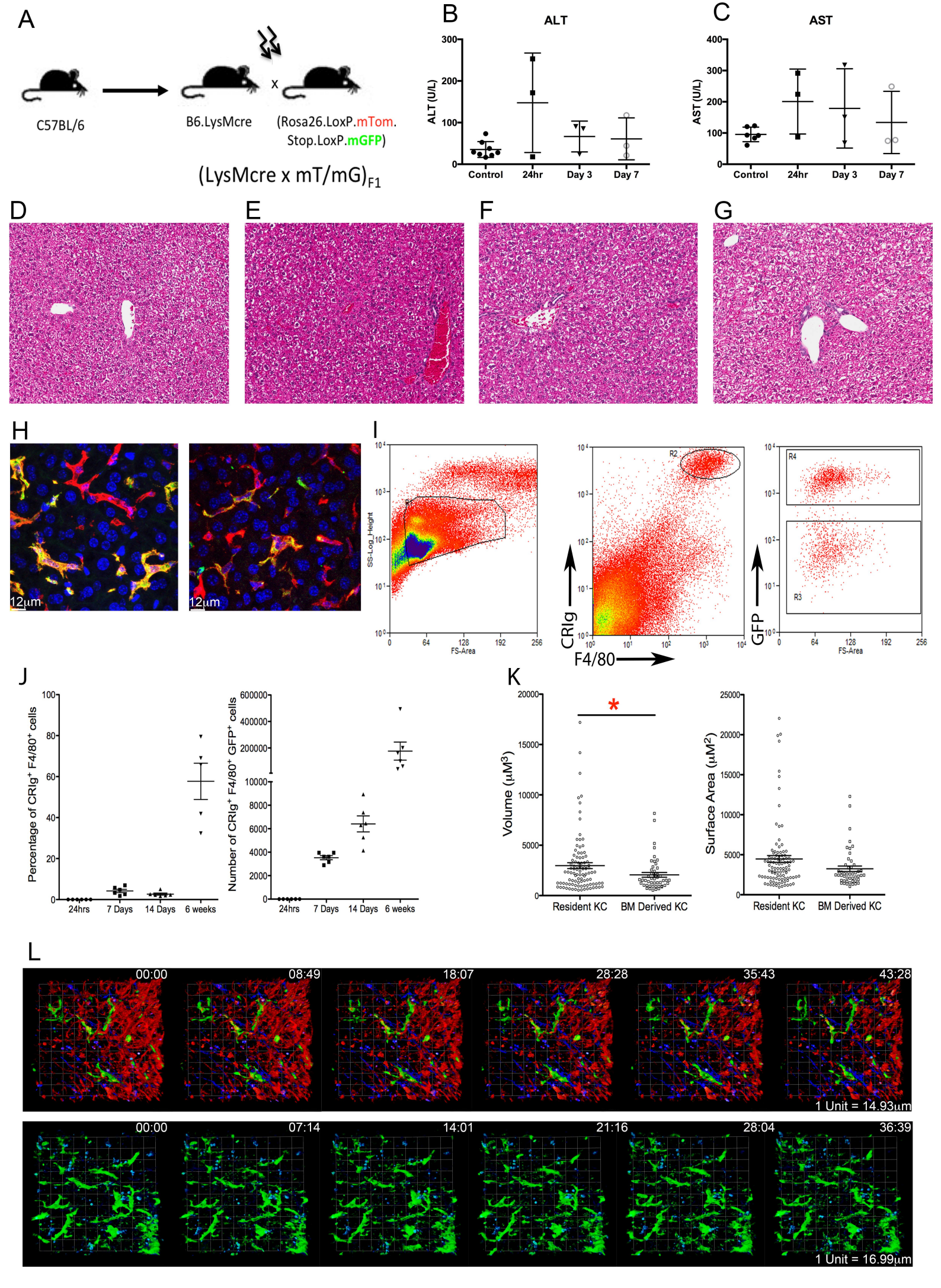
A
C57BL/6
B6.LysMcre
x
(Rosa26.LoxP.mTom.
Stop.LoxP.mGFP)
(LysMcre x mT/mG)F1
B
ALT
ALT (U/L)
300
200
100
0
Control
24hr
Day 3
Day 7
C
AST
AST (U/L)
400
300
200
100
0
Control
24hr
Day 3
Day 7
D
E
F
G
H
12µm
12µm
I
SS-Log_Height
FS-Area
R2
CRIg
F4/80
R4
R3
GFP
FS-Area
J
Percentage of CRIg+ F4/80+ cells
24hrs
7 Days
14 Days
6 weeks
Number of CRIg+ F4/80+ GFP+ cells
24hrs
7 Days
14 Days
6 weeks
K
*
Volume (µM3)
Resident KC
BM Derived KC
Surface Area (µM2)
Resident KC
BM Derived KC
L
00:00
08:49
18:07
28:28
35:43
43:28
1 Unit = 14.93µm
00:00
07:14
14:01
21:16
28:04
36:39
1 Unit = 16.99µm

Figure 2

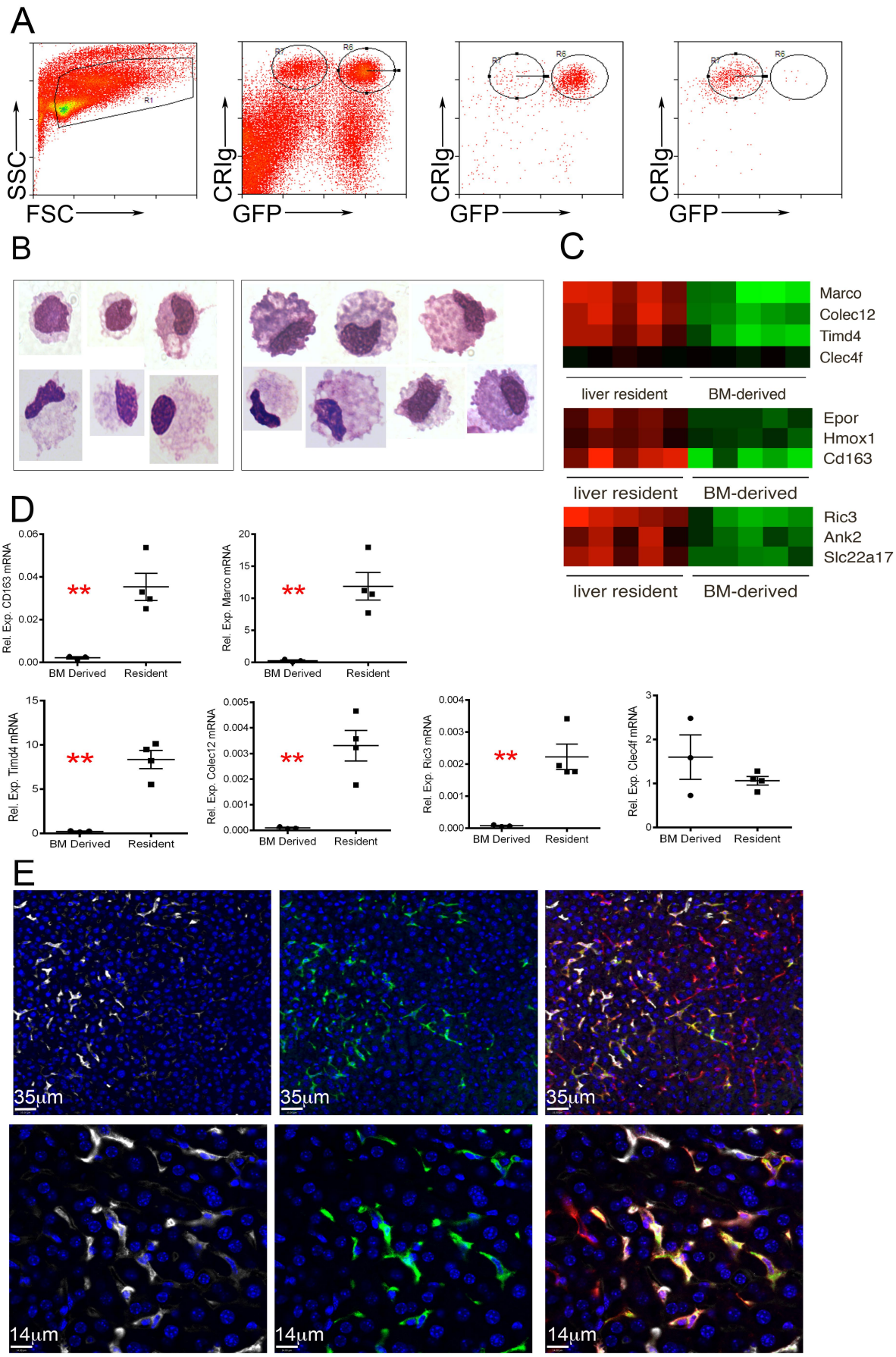
A
SSC
FSC
R1
CRIg
GFP
R7
R6
B
C
Marco
Colec12
Timd4
Clec4f
liver resident
BM-derived
Epor
Hmox1
Cd163
Ric3
Ank2
Slc22a17
D
Rel. Exp. CD163 mRNA
Rel. Exp. Marco mRNA
Rel. Exp. Timd4 mRNA
Rel. Exp. Colec12 mRNA
Rel. Exp. Ric3 mRNA
Rel. Exp. Clec4f mRNA
BM Derived
Resident
**
E
35μm
14μm

Figure 3

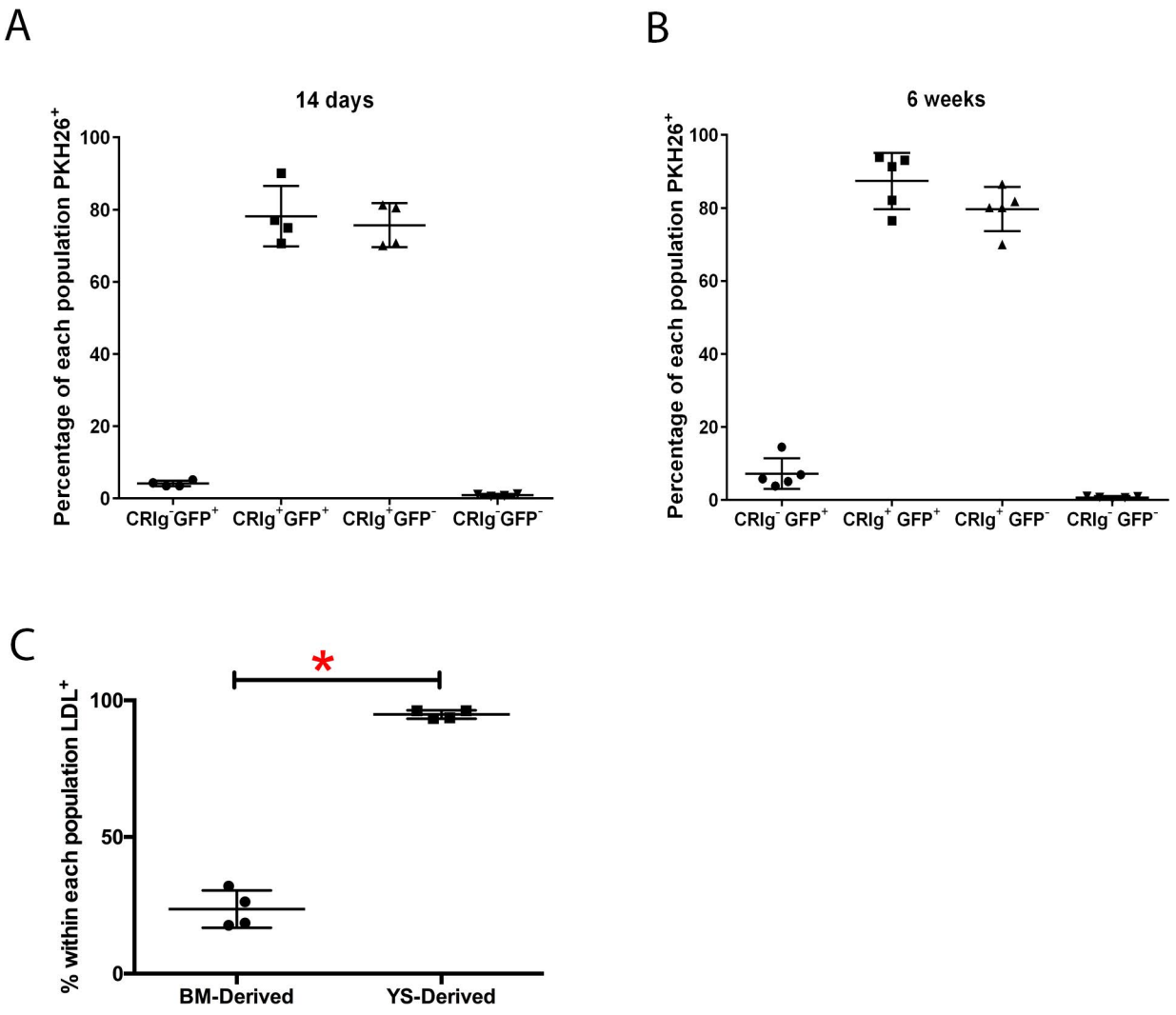
A
14 days
Percentage of each population PKH26+
100
80
60
40
20
0
CRIg-GFP+
CRIg+GFP+
CRIg+GFP-
CRIg-GFP-
B
6 weeks
Percentage of each population PKH26+
100
80
60
40
20
0
CRIg- GFP+
CRIg+ GFP+
CRIg+ GFP-
CRIg- GFP-
C
*
% within each population LDL+
100
50
0
BM-Derived
YS-Derived

Figure 4

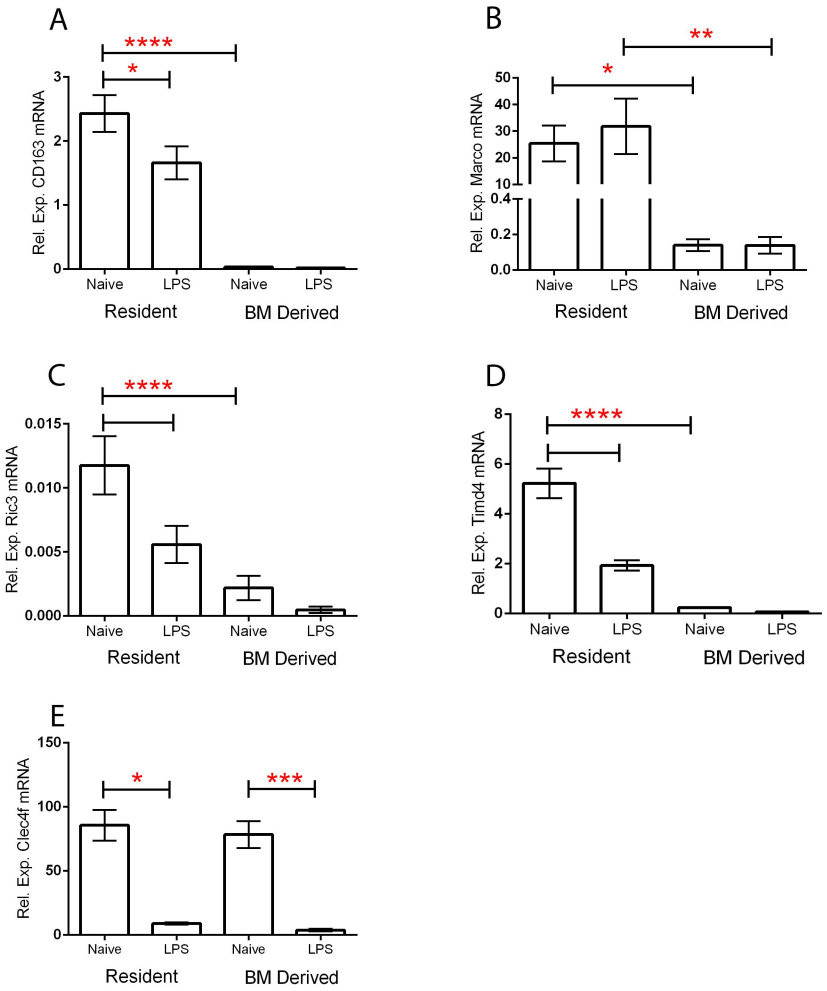
A
****
*
Rel. Exp. CD163 mRNA
3
2
1
0
Naive
LPS
Naive
LPS
Resident
BM Derived
B
**
*
Rel. Exp. Marco mRNA
50
40
30
20
10
0.4
0.2
0.0
Naive
LPS
Naive
LPS
Resident
BM Derived
C
****
Rel. Exp. Ric3 mRNA
0.015
0.010
0.005
0.000
Naive
LPS
Naive
LPS
Resident
BM Derived
D
****
Rel. Exp. Timd4 mRNA
8
6
4
2
0
Naive
LPS
Naive
LPS
Resident
BM Derived
E
*
***
Rel. Exp. Clec4f mRNA
150
100
50
0
Naive
LPS
Naive
LPS
Resident
BM Derived

Figure 5

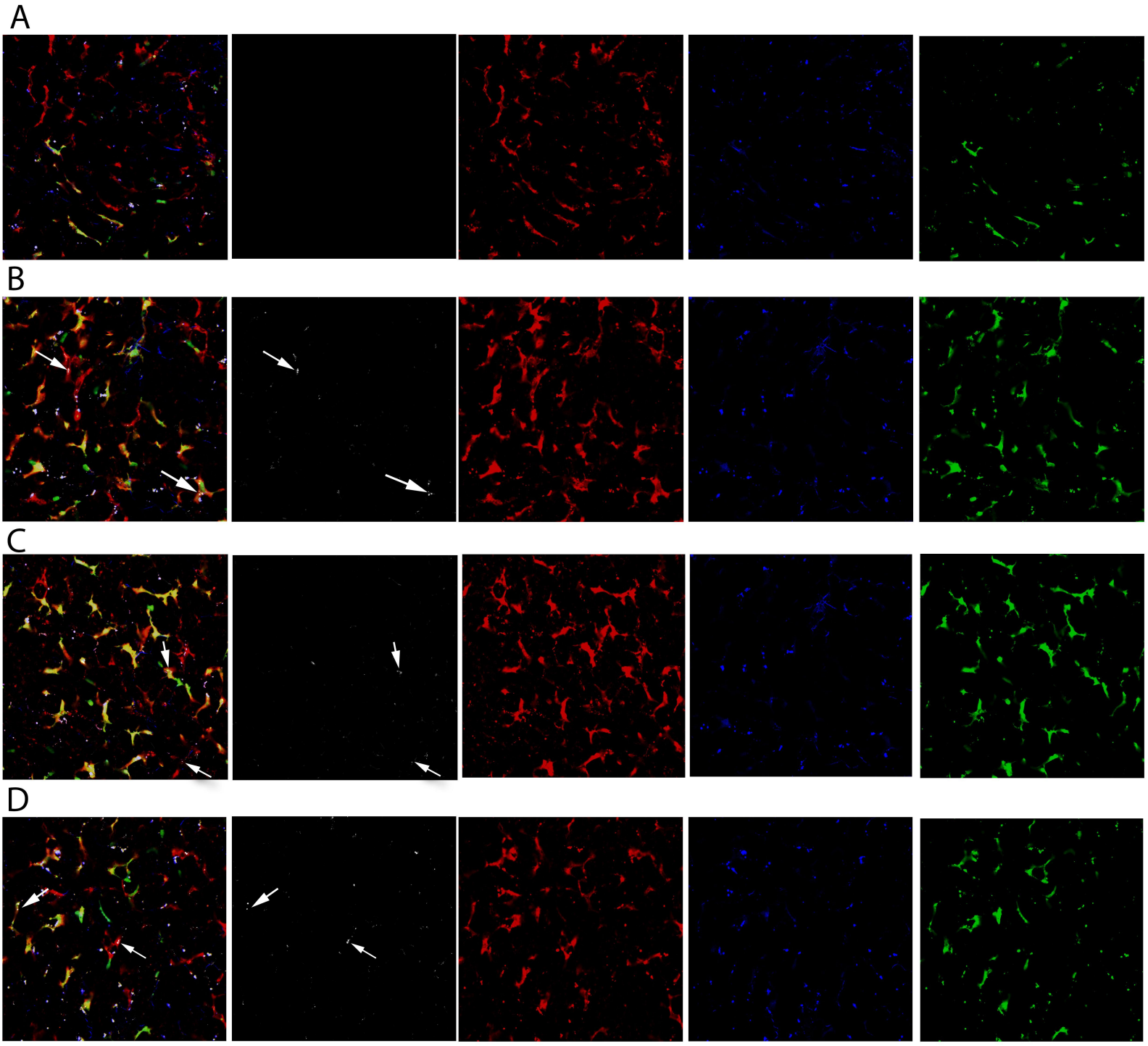
A
B
C
D

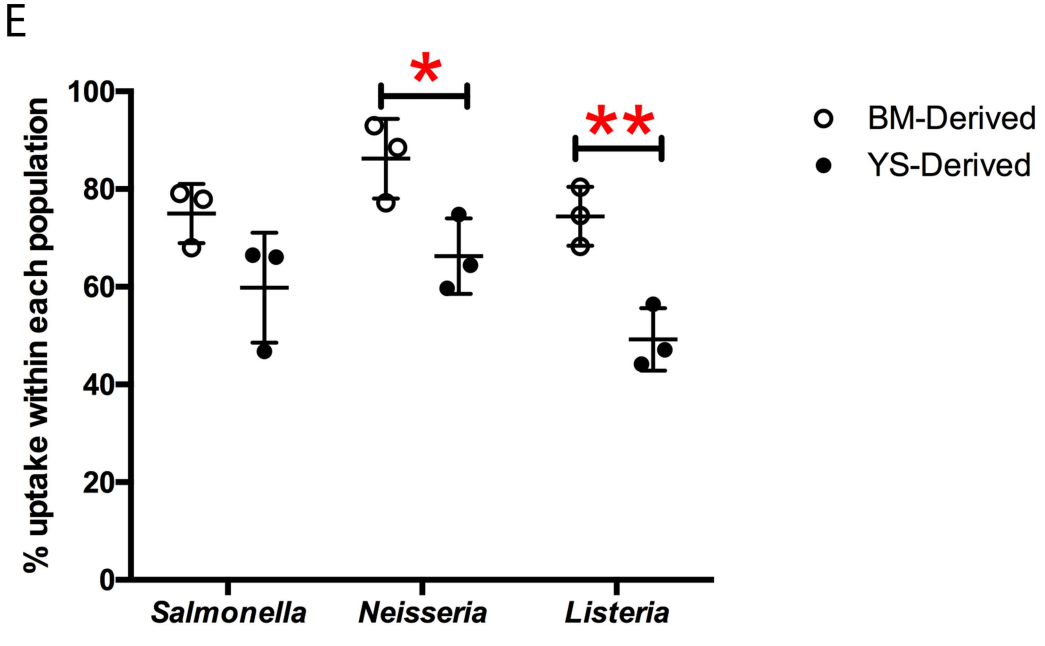
E
% uptake within each population
100
80
60
40
20
0
*
**
BM-Derived
YS-Derived
Salmonella
Neisseria
Listeria

Figure 6

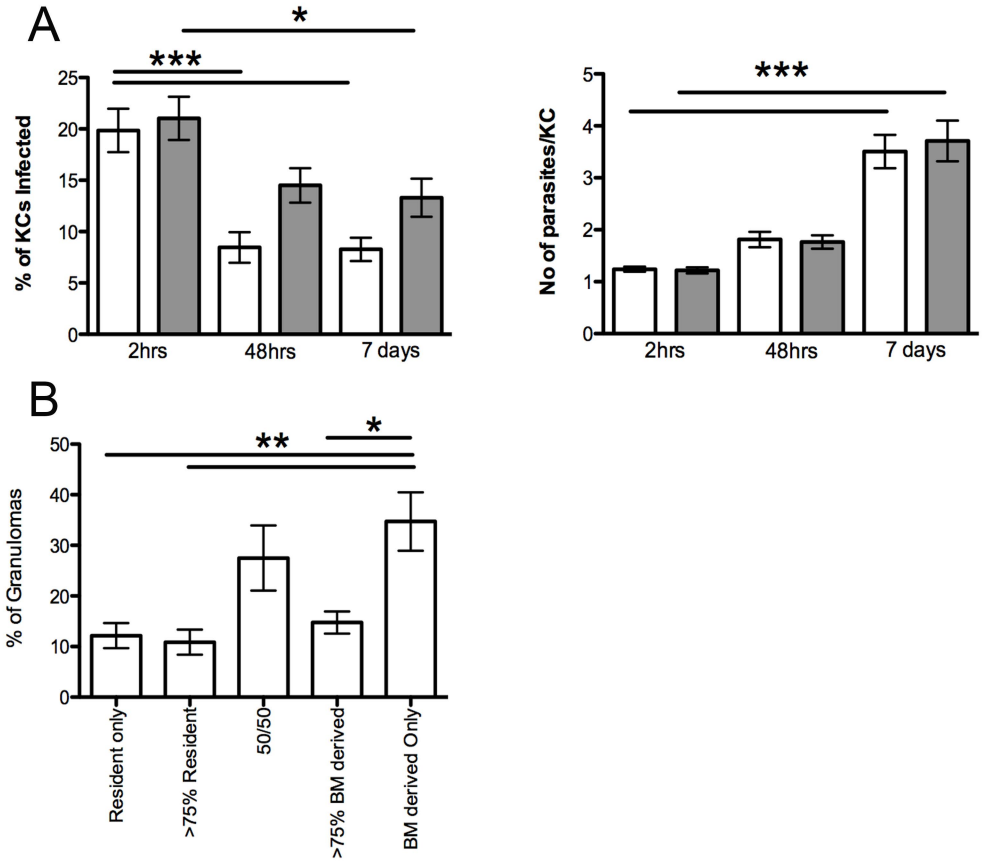
A
*
***
% of KCs Infected
25
20
15
10
5
0
2hrs
48hrs
7 days
***
No of parasites/KC
5
4
3
2
1
0
2hrs
48hrs
7 days
B
**
*
% of Granulomas
50
40
30
20
10
0
Resident only
>75% Resident
50/50
>75% BM derived
BM derived Only

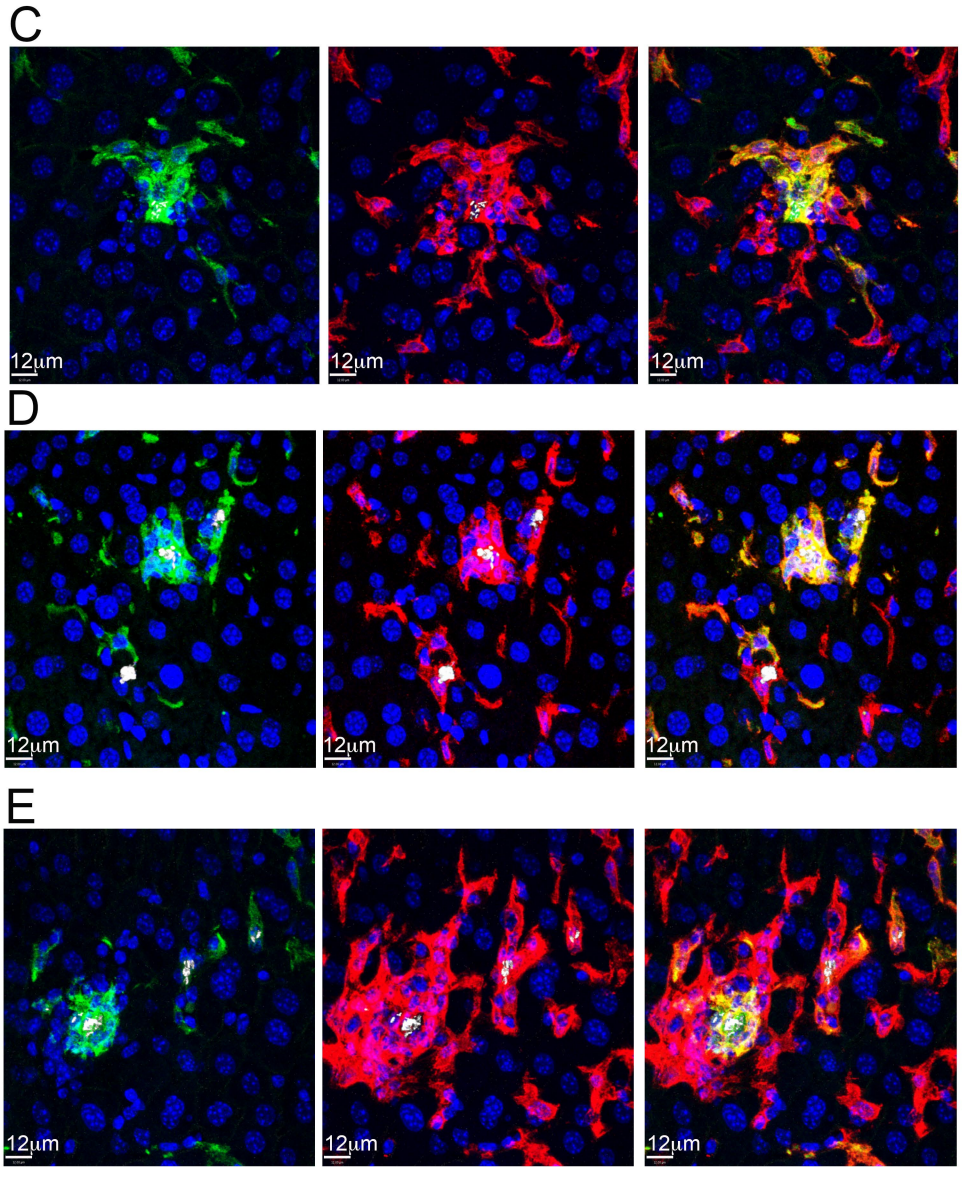
C
12µm
12µm
12µm
D
12µm
12µm
12µm
E
12µm
12µm
12µm

Liver Macrophage Function is Guided by Micro-environment rather than Origin.

Lynette Beattie[1,3], Amy Sawtell[1], Jason Mann[1], Teija CM Frame[3], Bianca Teal[3], Fabian de Labastida Rivera[3], Najmeeyah Brown[1], Katherine Walwyn-Brown[1], John W.J. Moore[1], Sandy MacDonald[2], Eng-Kiat Lim[1], Jane E Dalton[1], Christian R Engwerda[3], Kelli P MacDonald[3] and Paul M. Kaye[1]*

Table of Contents:

Methods:

Mice and Infection

C57BL6 or B6.CD45.1 mice were obtained from Charles River (UK) or the Australian Resource Centre (WA). mT/mG [1], lysMcre [2] and B6.MacGreen [3] mice have been previously described. Mice were bred and housed under specific pathogen-free conditions and used at 6–12 weeks of age. The Ethiopian strain of *Leishmania donovani* (LV9) and tandem Tomato fluorescent protein expressing LV9 (tdTom.LV9) [4] were maintained by serial passage in Rag-$1^{-/-}$ mice. Amastigotes were isolated from infected spleens [5], and mice were infected with $3x10^7$ *L. donovani* amastigotes intravenously (i.v.) via the tail vein in 200μl of RPMI 1640 (GIBCO, UK). For the generation of chimeras, mice were placed on acidified water for at least 2 days prior to irradiation. Donor mice were irradiated with 1100 rads on a split-dose regimen (550 rads per dose, 24hours apart) and were then reconstituted with 2-$5x10^6$ donor bone marrow cells via tail vein injection. Reconstituted mice were treated with oral antibiotics (Baytril) for 4 weeks post-reconstitution.

Liver enzyme analysis

Heparinized blood was immediately centrifuged for 10 min at 300 × *g*. Plasma was stored at -80^{o}C until analysis. Alanine aminotransferase (ALT) and aspartate transaminase (AST) levels were determined using a Beckman Unicell DxC800 analyzer in a single batch.

Image Analysis

For 4D analysis, 20-35μM Z stacks were acquired with a Z distance of 2μM approximately every 15-30sec. Data were rendered and analysed using Volocity software (Perkin Elmer) and cell analysis performed automatically with manual checking as previously described [6].

Confocal Microscopy

Confocal microscopy was performed on 20μm frozen sections. For tissue containing tdTom expressing parasites, tissues were fixed in 4% paraformaldehyde (PFA) for two hours before overnight incubation in 30% sucrose and embedding in OCT medium (Sakura). Antibodies were conjugated to Alexa488 or Alexa647 (eBioscience, UK). Slides were blinded before imaging on a Zeiss LSM510 axioplan microscope (Carl Zeiss Microimaging). Data were rendered and analysed using Volocity software (Improvision).

Flow cytometry and cell sorting

Hepatic mononuclear cells were prepared from the livers of chimeric mice. 20 chimeric mice were used for the microarray study. We conducted five independent sorts to generate samples for analysis. For each sorting experiment (n=4 mice), we isolated both YS-derived and BM-derived KC from liver mononuclear cells that were pooled prior to sorting. 3 of the experiments were performed on chimeric mice that contained GFP^+ liver resident KCs and 2 experiments were performed on chimeric mice that contained GFP^+ BM derived KCs. To isolate liver mononuclear cells, livers were perfused with 0.4mg/mL of warmed liberase TL (Roche) then removed, homogenised with a scalpel blade and digested at 37^oC for 45min. Digested livers were passed over 100μM cell strainers, washed in PBS containing 2%FCS and resuspended in 33% percoll for centrifugation at 693g for 12min. The remaining cell pellet was kept for further analysis. Isolated cells were blocked with anti CD16/32 then labelled with F4/80-Alexa488, GR-1 PeCy7 (eBioscience) and CRIg (clone 14G6, Helmy Cell 2006, provided by Genentech Inc) that was conjugated to Atto 647H via lightning-link

conjugation (Innova Biosciences). Cells were sorted on a MoFlo cell sorter (DAKO) based on expression of cell surface markers and GFP. Sorted cells were pelleted and resuspended in Trizol (Invitrogen). A small fraction of cells (approximately 3000 sorted cells) were spun onto glass slides, fixed in methanol and stained with Giemsa for morphological analysis.

Real-time PCR

Purified cells were resuspended and frozen in QIAZOL lysis buffer. RNA was isolated using a miRNA easy kit (QIAGEN). RNA was reverse transcribed into cDNA with a Superscript III first-strand synthesis kit (Invitrogen). Real-time quantitative PCR was performed with Fast SYBR green PCR master mix in a StepOne Plus Real-Time PCR system (Applied Biosystems). Accumulation of target genes was normalized to HPRT, (results were the same if normalised to β-actin [7] or ribosomal protein L32 [8]) and expressed as relative expression via the change in cycle threshold (ΔΔCT) analysis method (relative expression in test sample versus RPMI controls). Oligonucleotides used for the specific amplification of target genes were; Timd-4: AGAATGTGCGCTTGGAGCTGAG/GGTTGGGAGAACAGATGTGGTC, CD163: GGCTAGACGAAGTCATCTGCAC/CTTCGTTGGTCAGCCTCAGAGA, Colec12: ACTCCAAGCACGGTCAGCTCAT/CTTGTTGCCAGTTGGACCAGGT, Ric3: GGTAGTGGAAGAGGACTGATGG/AGTGGAGCAGTTCCGATCCTCT, Clec4f: TCACAGCCTTGGAGACCTGAGT/CCTAAGCCTCTGGATAGCCACT, MARCO: ATGGCACCAAGGGAGACAAAGG/GCCTGGTTTTCCAGCATCACCT.

RBC Phagocytosis

BM chimeric mice were generated as described above. Two or six weeks post irradiation and bone marrow transplantation, desialyated and labelled red blood cells were transferred IV as described [9]. Briefly, normal mouse red blood cells were labelled with 2-mM solution of PKH-26 (Sigma) for 5min at 25^{o}C. The labelled cells were then treated with 0.012U of *Arthrobacter ureafaciens* and *Vibrio cholera* neuraminidases (Sigma) for 1hr at 37^{o}C. A chimeric mouse that received no red blood cell injection was used as a control.

LPS Treatment

BM chimeric mice were generated as described above with C57BL/6 recipients and B6.CD45.1 donors. Six weeks after bone marrow transplant, the recipient mice were injected with 100ug LPS (Sigma) intravenously. 24hrs post-injection, the mice were sacrificed, and the livers prepared for cell sorting as described above. KCs were sorted based on expression of CD45.1/.2, CRIg and F4/80.

In Vivo Bacterial Uptake Assay

Salmonella enterica subspecies *enterica* serovar Typhimurium (*S*. typhimurium), *Neisseria meningitidis* or *Listeria monocytogenes* were grown to an optical density of 0.8 and 600nm and then washed and heat-killed for 2hrs at 60^{o}C and stored at 4^{o}C until use. Heat-killed bacteria were labelled with SYTO 62 (Molecular Probes) for 30 mins at RT. Labelled bacteria were injected intravenously into the tail vein of B6.MacGreen → B6.CD45.1 chimeric mice, and the livers removed after 2 hours. Whole, unfixed liver tissue was imaged on a Zeiss 780 NLO 2-photon microscope (Carl Zeiss Microimaging). Images were acquired with a 40x 1.1 water immersion objective and fluorescence excitation provided by a

Chameleon XR Ti:sapphire laser (Coherent) tuned to 900nm. For quantitation via flow cytometry, hepatic mononuclear cells were prepared and samples labelled with F4/80 (PE) (BioLegend) before acquisition using a BD LSR Fortessa (BD). SYTO 62 was detected in the APC (R670/14) channel. Data was analysed using FlowJo v10 OSX software (Treestar, Oregon).

Uptake of acetylated LDL

Hepatic mononuclear cells were prepared from B6.MacGreen → B6.CD45.1 chimeric mice (8 mice, 4 pools of 2 livers) and depleted of B and T cells using EasySep mouse biotin selection kit (Stemcell Technologies). Samples were labelled with F4/80 (PE-Cy7), CD11b (PerCP-Cy5.5), CD45.1 (PE), CD45.2 (AF700) and Tim4 (AF647) and then incubated with 10μg/mL Alexa Flour 594 AcLDL (Molecular Probes) for 1 hr at 37^{o}C. Flow cytometry acquisition was performed using a BD LSR Fortessa (BD) and data was analysed using FlowJo v10 OSX software (Treestar, Oregon).

Supplementary Table 1:

Gene Ontology terms over-represented in the analysis of genes expressed by YS-derived but not BM-derived KCs.

GO ACCESSION	GO Term	p-value	Count in Selection
GO:0055065	metal ion homeostasis	0.0002	5
GO:0055080	cation homeostasis	0.0003	5
GO:0034394	protein localization to cell surface	0.0003	2
GO:0050801	ion homeostasis	0.0004	5
GO:0006875	cellular metal ion homeostasis	0.0010	4
GO:0006897|GO:0016193|GO:0016196	endocytosis	0.0014	4
GO:0030003	cellular cation homeostasis	0.0014	4
GO:0004900	erythropoietin receptor activity	0.0015	1
GO:0004411	homogentisate 1,2-dioxygenase activity	0.0015	1
GO:0033292	T-tubule organization	0.0015	1
GO:0006873	cellular ion homeostasis	0.0017	4
GO:0005044	scavenger receptor activity	0.0018	2
GO:0048878	chemical homeostasis	0.0019	5
GO:0055082	cellular chemical homeostasis	0.0023	4
GO:0006788	heme oxidation	0.0030	1
GO:0031783	type 5 melanocortin receptor binding	0.0030	1
GO:0086036	regulation of cardiac muscle cell membrane potential	0.0030	1
GO:0005686	U2 snRNP	0.0030	1
GO:0036017	response to erythropoietin	0.0030	1
GO:0004392	heme oxygenase (decyclizing) activity	0.0030	1
GO:0036018	cellular response to erythropoietin	0.0030	1
GO:0032764	negative regulation of mast cell cytokine production	0.0030	1
GO:0038162	erythropoietin-mediated signaling pathway	0.0030	1
GO:0070436	Grb2-EGFR complex	0.0030	1
GO:0031780|GO:0071856	corticotropin hormone receptor binding	0.0030	1
GO:0055072	iron ion homeostasis	0.0032	2
GO:0038024	cargo receptor activity	0.0035	2
GO:0015891|GO:0015892	siderophore transport	0.0045	1
GO:0032763	regulation of mast cell cytokine production	0.0045	1
GO:0015688	iron chelate transport	0.0045	1
GO:0070996	type 1 melanocortin receptor binding	0.0045	1
GO:0033212	iron assimilation	0.0045	1
GO:0042167	heme catabolic process	0.0045	1
GO:0033214	iron assimilation by chelation and transport	0.0045	1
GO:0004566	beta-glucuronidase activity	0.0045	1
GO:0046149	pigment catabolic process	0.0045	1
GO:0019725	cellular homeostasis	0.0047	4
GO:0006909	phagocytosis	0.0051	2
GO:0006874	cellular calcium ion homeostasis	0.0054	3

GO:0086018	SA node cell to atrial cardiac muscle cell signalling	0.0060	1
GO:0086015	SA node cell action potential	0.0060	1
GO:0031781	type 3 melanocortin receptor binding	0.0060	1
GO:0043305	negative regulation of mast cell degranulation	0.0060	1
GO:0033015	tetrapyrrole catabolic process	0.0060	1
GO:0006787	porphyrin-containing compound catabolic process	0.0060	1
GO:0031782	type 4 melanocortin receptor binding	0.0060	1
GO:0031779	melanocortin receptor binding	0.0060	1
GO:0055074	calcium ion homeostasis	0.0062	3
GO:0072503	cellular divalent inorganic cation homeostasis	0.0063	3
GO:0055076	transition metal ion homeostasis	0.0066	2
GO:0055001	muscle cell development	0.0073	2
GO:0072507	divalent inorganic cation homeostasis	0.0073	3
GO:0005134	interleukin-2 receptor binding	0.0075	1
GO:0001537	N-acetylgalactosamine 4-O-sulfotransferase activity	0.0075	1
GO:2000369	regulation of clathrin-mediated endocytosis	0.0075	1
GO:0033007	negative regulation of mast cell activation involved in immune response	0.0075	1
GO:0044183	protein binding involved in protein folding	0.0075	1
GO:0002246	wound healing involved in inflammatory response	0.0075	1
GO:0006572	tyrosine catabolic process	0.0075	1
GO:0071276	cellular response to cadmium ion	0.0075	1
GO:0005685	U1 snRNP	0.0075	1
GO:0086070	SA node cell to atrial cardiac muscle cell communication	0.0075	1
GO:0045766	positive regulation of angiogenesis	0.0080	2
GO:0005581	collagen	0.0080	2
GO:0043619	regulation of transcription from RNA polymerase II promoter in response to oxidative stress	0.0090	1
GO:0006559	L-phenylalanine catabolic process	0.0090	1
GO:0071243	cellular response to arsenic-containing substance	0.0090	1
GO:1902222	erythrose 4-phosphate/phosphoenolpyruvate family amino acid catabolic process	0.0090	1
GO:0004630	phospholipase D activity	0.0090	1
GO:0006954	inflammatory response	0.0093	3

[1] Muzumdar MD, Tasic B, Miyamichi K, Li L, Luo L. A global double-fluorescent Cre reporter mouse. Genesis 2007;45:593-605.
[2] Clausen BE, Burkhardt C, Reith W, Renkawitz R, Forster I. Conditional gene targeting in macrophages and granulocytes using LysMcre mice. Transgenic Res 1999;8:265-277.
[3] Sasmono RT, Oceandy D, Pollard JW, Tong W, Pavli P, Wainwright BJ, et al. A macrophage colony-stimulating factor receptor-green fluorescent protein transgene is expressed throughout the mononuclear phagocyte system of the mouse. Blood 2003;101:1155-1163.
[4] Beattie L, Peltan A, Maroof A, Kirby A, Brown N, Coles M, et al. Dynamic imaging of experimental Leishmania donovani-induced hepatic granulomas detects Kupffer cell-restricted antigen presentation to antigen-specific CD8 T cells. PLoS pathogens 2010;6:e1000805.
[5] Smelt SC, Engwerda CR, McCrossen M, Kaye PM. Destruction of follicular dendritic cells during chronic visceral leishmaniasis. J Immunol 1997;158:3813-3821.
[6] Beattie L, d'El-Rei Hermida M, Moore JW, Maroof A, Brown N, Lagos D, et al. A transcriptomic network identified in uninfected macrophages responding to inflammation controls intracellular pathogen survival. Cell host & microbe 2013;14:357-368.
[7] Shih VF, Davis-Turak J, Macal M, Huang JQ, Ponomarenko J, Kearns JD, et al. Control of RelB during dendritic cell activation integrates canonical and noncanonical NF-kappaB pathways. Nature immunology 2012;13:1162-1170.
[8] Reis BS, Rogoz A, Costa-Pinto FA, Taniuchi I, Mucida D. Mutual expression of the transcription factors Runx3 and ThPOK regulates intestinal CD4(+) T cell immunity. Nature immunology 2013;14:271-280.
[9] Bratosin D, Estaquier J, Ameisen JC, Aminoff D, Montreuil J. Flow cytometric approach to the study of erythrophagocytosis: evidence for an alternative immunoglobulin-independent pathway in agammaglobulinemic mice. Journal of immunological methods 2002;265:133-143.